Detection of Air Leakage in Building Envelopes using Microphone Arrays

Benedikt Kölsch[1], Björn Schiricke[2], Eckhard Lüpfert[2] and **Bernhard Hoffschmidt[2]**

[1]Institute of Solar Research, German Aerospace Center (DLR), Karl-Heinz-Beckurts-Str. 13, 52428, Jülich, Germany

[2] Institute of Solar Research, German Aerospace Center (DLR), Linder Höhe, 51147, Cologne, Germany

ABSTRACT

Unintended airflow through building envelopes leads to an increased demand in heating and cooling energy. The most common way to measure air leakage of buildings is the blower door test, which quantifies the overall leakage rate of one room or a building. To reduce air leakage and associated energy loss in new and existing buildings, it is necessary to identify leak locations and prioritize sealing of more substantial leaks. However, detection and quantification of individual leaks with smoke tracers or infrared thermography are challenging, time-consuming, and depend on the operator's experience.

Acoustic methods have been identified to have the potential to localize and quantify individual leaks without the need for pressure or temperature differences. In this work, the acoustic beamforming method is proposed using a microphone array to detect leak locations and visualize them (acoustic camera). The objective of this investigation is to identify the potential of this technique for application to building envelopes. A pair of omnidirectional speakers is placed as a sound generator inside a room, and the microphone ring array with 48 microphones outside. As an experimental setup, cable ties are wedged in a window frame to simulate a damaged window gasket and to create reproducible leaks of different sizes at the same place. Overlay of an optical picture with the acoustic image obtained from beamforming enables the visualization of leaks of sound through the building envelope. All experiments were conducted using white noise with an analyzed frequency range of 1-25 kHz. The sound sources are evaluated at multiple third-octave bands within this frequency range, enabling a distinction between these leaks at different frequencies.

INTRODUCTION

In addition to quantifying leaks in the building envelope, it is crucial to identify leak locations. The knowledge of leak locations enables prioritizing sealing of more substantial leaks to reduce air leakage and associated energy loss in new and existing buildings (Walker and Wilson 1998). Identifying single leaks in the building envelope is challenging, time-consuming, and depends on the operator's experience. Leak locations may be identified using, e.g., smoke sticks or anemometers in conjunction with a fan pressurization measurement, infrared thermography, or tracer gas. However, smoke sticks and anemometers require a pressure difference to detect leaks. The use of infrared thermography requires a temperature gradient across the building envelope in addition to a pressure difference. Acoustic methods have been identified to have the potential to localize (Raman et al. 2014) and quantify (Kölsch et al. 2021) individual leaks without the need for pressure or temperature differences. In this paper, an acoustic beamforming method is proposed using a microphone array to detect leak locations and visualize them. This investigation aims to identify the potential of this technique for an

application to building envelopes. This paper shall demonstrate that sound, transmitted through small leaks in a building enclosure, can be localized using a microphone array with the corresponding signal analysis called beamforming. In addition to Raman et al. (Raman et al. 2014), this paper investigates much smaller leaks and higher frequencies.

FUNDAMENTALS

The physical principle of sound source localization is successfully performed by humans and animals to estimate the direction and distance of surrounding sound sources. The interaural time difference (ITD) of sound in combination with the interaural level differences (ILD) between both ears enables localizing and differentiating even multiple sound sources (Moore 2004). The theoretical knowledge for transforming this into a technical application using microphone arrays is known for decades (Billingsley and Kinns 1976). However, only within the last twenty years, the necessary computing power got available to process multiple microphone signals at high frequency simultaneously, making this principle usable for practical applications. There are a few different microphone array measurement techniques for the identification or localization of sound sources. The most common one is the beamforming technique, besides others such as the acoustic holography (Maynard, Williams, and Lee 1985) and the inverse boundary element method (Bi et al. 2019). Today, these techniques of sound source localization are commonly used in the automotive, railroad, or aerospace sector to detect significant noise and sound sources of vehicles and reduce them.

Beamforming is a signal processing technique that enables an array of microphones to separate sound sources from different directions (Herbordt 2005). The measuring principle is based on the fact that the microphone array focuses on different measuring points on the measured object. During the analysis, the time signals from the array's microphones are superimposed with a time delay corresponding to the time the sound wave takes from the focused point to the individual microphones. These time-shifted signals from all microphones are summed, resulting in a time signal assigned to the respective focus point. If a noise component's origin is found at that focus point, there is positive interference for all microphone signals and, therefore, a maximum summed signal level. Otherwise, partial cancellation of the microphone signals results in lower summed signal levels. The system is called an "acoustic camera" because the result of the scan process over a range of viewing angles and their focal distances produces an image of the most intensive constructive interferences of the acoustic waves in the microphone array. The advantage for a wide range of applications is the visual (2D) result of the scene, which is typically overlaid on a visible image of the same scene for interpretation.

Beamforming

The most straightforward calculation is the delay-and-sum beamforming in the time domain applied for this work. Every time function for each focus point $\vec{x}$ can be constructed as (Jaeckel 2006):

$$\hat{f}(\vec{x}, t) = \frac{1}{M} \sum_{i=1}^{M} f_i(t - \Delta_i) \tag{1}$$

M is the number of microphones in the chosen array, and $f_i(t)$ are the time signals of the sound pressure recorded at each individual microphone i. The time delays Δ_i for each microphone signal are calculated run times over all microphones between the focus point $\vec{x}$ and the microphone i. Imprecisely known location of the focus points leads to an error in evaluating the calculated sound pressure levels (focusing error), which can be a problem for non-stationary sound sources. The magnitude of this error

depends on the frequency and chosen microphone array geometry. This fundamental principle of delay-and-sum calculation is illustrated in Fig. 1 a) for a simplified array of four microphones.
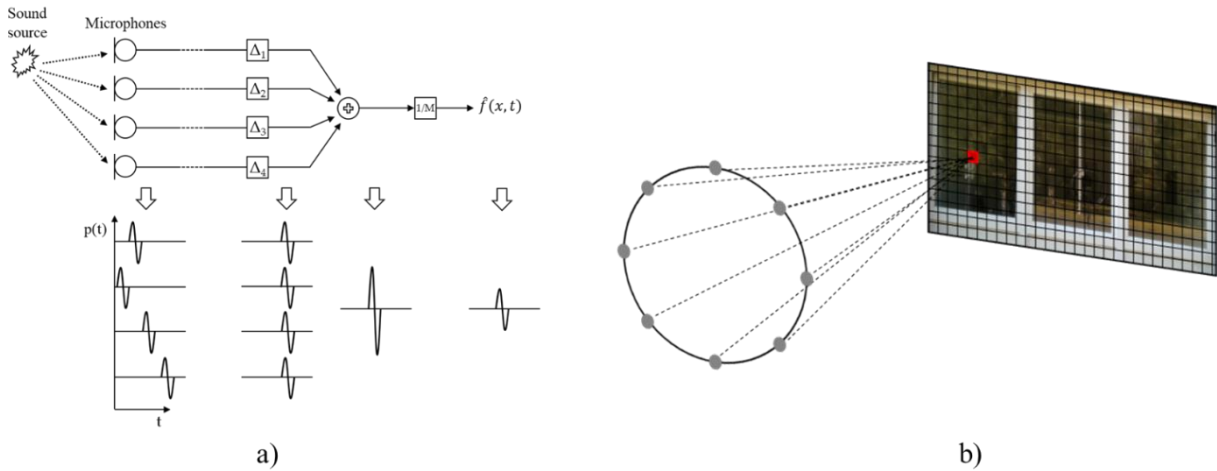

Figure 1 a) Basic principle of delay-and-sum beamforming in the time domain with a simplified microphone array, based on (Jaeckel 2006), b) Scanning process

The effective sound pressure $\hat{p}_{rms}(\vec{x})$ at the calculated focus point can finally be calculated as:

$$\hat{p}_{rms}(\vec{x}) \approx \hat{p}_{rms}(\vec{x}, n) = \sqrt{\frac{1}{n} \sum_{k=0}^{n-1} \hat{f}^2(\vec{x}, t_k)} \tag{2}$$

where n is the total number of corresponding discrete time samples, and t_k the time value at the sample index k.

During the signal analysis, the focus point $\vec{x}$ is scanned on a defined grid (Fig. 1 b)). The individual sound pressure values $\hat{p}_{rms}(\vec{x})$ from the microphones array signals can be assigned to the pixels of the optical camera image of the same scene. The sound sources are visualized by superimposing acoustic values $\hat{p}_{rms}(\vec{x})$ as colors on the optical camera image.

The possible frequency range to be examined depends on the following factors: a lower cut-off frequency is limited by the size of the microphone array; the larger the array, the lower its cut-off frequency. The upper cut-off frequency is determined by the signal sampling frequency and the distances between the microphones. If the distance between the microphones is larger than half of the analyzed wavelength, sound sources might not be located correctly.

Microphone Array Directivity

The degree to which other sound sources outside the focus direction are suppressed depends on the chosen array geometry and size. This effect can be evaluated by the beam pattern of an array. A beam pattern plot evaluates the magnitude of an array output as a function of the incoming viewing angle of sound waves with regard to the focus direction. The array directivity is often characterized by a single frequency wave from an arbitrary incident angle (Grythe 2015b). A detailed derivation of the underlying equations can be found in Ref. (Teutsch 2007).

METHODOLOGY

Measurement Equipment and Experimental Setup

In the following experiments, the test site is a small office at ground level with a window façade (one wall) as part of the building envelope. A microphone ring array with 48 equally spaced microphones and a diameter of 0.75 m (GFaI tech - ACPro 48) is placed outside the building in front of the window façade. The array remained stationary during the measurements, and the distance between microphone array and object was 2.3 m. The recommended frequency range of this array lies between 0.164 and 20 kHz. According to the manufacturer, if the sound source localization is more important than the absolute value of the sound pressure level, measurements up to 60 kHz are feasible. In the center of the array, a video camera (Intel RealSense Depth Camera D435) is located to record an optical image (1920 x 1080 pixels) of the scene. The measurement setup of the microphone array in front of the façade is displayed in Fig. 2a. A pair of high and mid/low-frequency omnidirectional speakers are placed inside the building in the middle of the office (Fig. 2b). The high-frequency speaker (Avisoft - ultrasonic omnidirectional dynamic speaker vifa) has an even frequency range of 15 to 120 kHz, and the low-frequency dodecahedron speaker (Infra Q-Sources Qohm) has an even frequency range of 0.05 to 16 kHz. A computer-generated broadband white noise was emitted at a level of 90 dB over a duration of 6 seconds. The sound waves generated by the speaker system penetrate through the leaks in the façade and are detected as individual sound sources by the acoustic camera system in the described scanning procedure. The data recorder (gfai mcdRec) records all microphone signals with a sampling frequency of 192 kHz and digitizes with 32 bit. The calculation of beamforming is performed by the software NoiseImage (GFaI 2020), and the visualization of the data is enabled with a Python script.

Acoustic measurements were performed with this microphone array for six different artificially constructed leaks. They are constructed using various combinations of cable ties wedged in the gasket of the right part (viewing from the outside) of the middle window to simulate a damaged window gasket and create leaks in a reproducible setup. Six combinations using two sizes of cable ties are used to create the leaks: a larger tie (top row of Fig. 3) with a width and thickness of 8 x 1.5 mm and a smaller one (bottom row of Fig. 3) with a width and thickness of 3 x 1 mm. To ensure the cable ties remain fix during the measurement, they are clamped onto a small piece of wood.
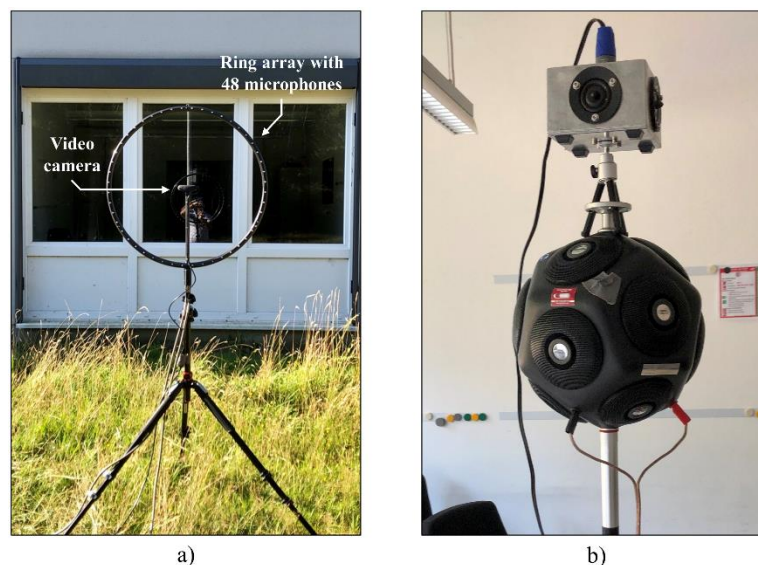

a)   b)

Figure 2 Setup of the microphone ring array and video camera in front of the building façade (a), speakers inside the building (b)
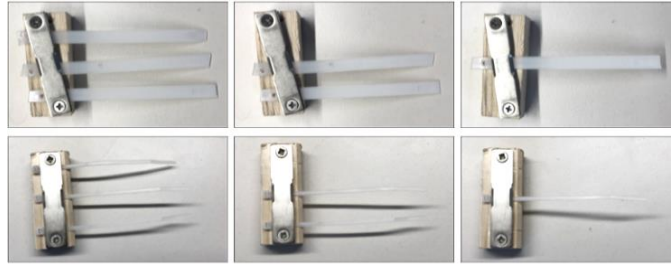
Figure 3 The two types of cable ties used to create reproducible artificial leaks in the window frame. Top row: large cable ties with an 8 mm width, bottom row: small cable ties with a 3 mm width

Analysis of Microphone Array Directivity

Directivity beam patterns of the used two-dimensional microphone ring array are calculated for three frequencies (1.25, 6.3, and 12.5 kHz) and illustrated in Fig. 4. These three frequencies show the differences in the directivity for the array at a low, mid, and high frequency. For this modeling, it is assumed that microphones are point-like and have individually perfect spherical directivity. The calculation of the beam patterns and visualization of all acoustic images are prepared in Python scripts.

The main lobe in the center corresponds to the array's focus direction. The side lobes do not correspond to the focus direction. The figures show to what extent sound sources outside the focus direction are reduced. The array's spatial resolution, and therefore the ability to separate sound sources, is determined by the width of the main lobe (Grythe 2015a). These calculations show how much the resolution increases with increasing frequency. The ratio between main and side lobes determines the contrast or dynamic range. In order to take advantage of the properties at different frequencies, broadband noise is applied for these measurements.
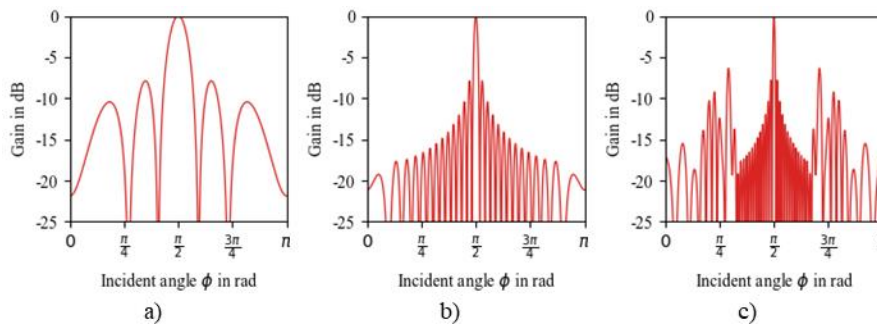

Figure 4 Modeled directivity patterns of the used microphone ring array at θ=π/2 for a) 1.25 kHz, b) 6.3 kHz, and c) 12.5 kHz

External Sound Source Reduction

As the sound source was placed inside the building and the microphones were placed outside, other disturbing sound sources (e.g., traffic, construction works, planes) are contained in the recorded signals, which is a significant difference to measurements under laboratory conditions. This may mask the intentional sound source from the building leaks. The building test site is located next to a street, a large construction site, and in the approach flight path of a large airport. Therefore, numerous external sound sources potentially disturb the acoustic measurements outside. In order to reduce the impact of unwanted noise in the recorded signal, a microphone signal next to the speaker inside the building is used as a reference signal. Based on a correlation analysis, the aim is to display only sources that significantly correlate with the recorded reference signal. This method is described in Refs. (Neugebauer, Rösel, and Döbler 2014; Döbler and Puhle 2015) with the application in wind tunnel experiments and enables to filter out and reduce the impact of unwanted noise on the measurement

results. All subsequent analyses use this signal filtering with the reference signal in order to reduce noise impact from the environment, which is implemented in the software NoiseImage (GFaI 2020).

RESULTS AND DISCUSSION

The following figures show the camera image of the examined window façade with the superimposed results of the beamforming analysis of the microphone array recorded from the white noise generated inside the building. Each pixel of the visible image is a focus point for the acoustic analysis where an effective sound pressure level is calculated, but only the shown range in dB is displayed.

To determine the detectability of the constructed leaks in the window gasket as a function of the frequency, the recorded white noise is analysed at various third-octave frequency bands. Fig. 5 shows images of four selected frequency bands with center frequencies of 1, 1.6, 6.3, and 20 kHz and a measurement with the largest constructed leak (three large cable ties (3 x 8 mm), top left configuration in Fig. 3) in the window gasket, which is clearly detected in all four selected frequency bands.

a) 1 kHz   b) 1.6 kHz   c) 6.3 kHz   d) 20 kHz
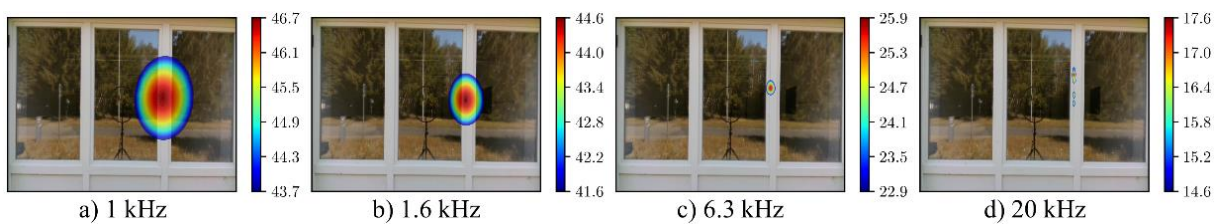
Figure 5 Acoustic images of selected third-octave frequency bands for the largest constructed leak of three 8 mm cable ties (3 x 8 mm) with superimposed sound pressure levels in dB

Only the highest 3 dB of the recorded sound pressure level is displayed to avoid a misleading interpretation of the results due to side lobes (see Fig. 4). The directional characteristic increases with increasing frequency, as already predicted in the previous section. At the highest displayed frequency band with a center frequency of 20 kHz, the sound source, identified as one single point source at lower frequencies, is detected as multiple separate small sources. Due to the construction of this leak with three clamped cable ties in the window gasket, the leak consists of two larger openings at the top and bottom of the cable tie row and two smaller openings between the ties. While Fig. 5 displays only four selected frequency bands for illustration purposes, this largest constructed leak is visible within almost the entire analyzed spectrum between 1 and 20 kHz. Fig. 6 shows the acoustical image of a third-octave frequency band of the same constructed leak with a center frequency of 5 kHz, where detection of the leak is not possible. In the acoustical image, several sound sources are equally distributed on the façade element underneath the window, and the constructed leak in the window gasket is now masked. The façade element below the window is made of thin plastic sheets in window frames. These sheets are vibrating in resonance, masking the measurement at the leak. This resonance is detected in all measurements with smaller leaks and shows the benefit of analyzing multiple frequency bands to increase the potential of correctly identifying possible leaks in the building enclosure.
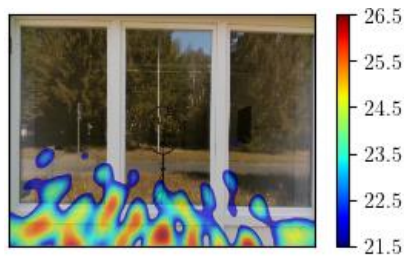
Figure 6 Acoustic image of resonance at 5 kHz frequency band for the largest constructed leak of three 8mm cable ties (3 x 8 mm) with superimposed sound pressure levels in dB

Figs. 7 and 8 show the acoustic images of selected frequency bands of the other constructed leak sizes (see Fig. 3 from large to small). The second-largest artificial constructed leak in Fig. 7 with two large cable ties are clamped in the gasket (2 x 8 mm) is visible almost across the entire spectrum as well. The difference compared to the largest leak configuration in Fig. 5 is a lower maximum sound pressure level of approximately 2 dB, which is significant.
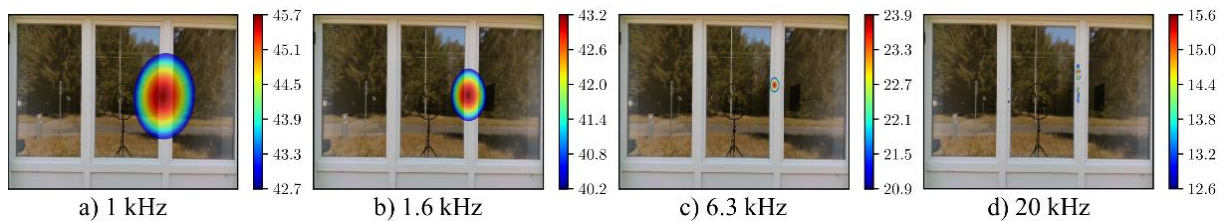

Figure 7 Acoustic images of selected third-octave frequency bands for the constructed leak of 2 x 8 mm with superimposed sound pressure levels in dB

In contrast to the measurements shown with large leaks in Figs. 5 and 7, where the leak's location can be observed almost in the entire frequency spectrum, in Fig. 8 the constructed leak is only visible at frequency bands above 16 kHz. The smaller the leaks, the lower the relevant signal level to be detected (see color bars). Due to the increased directivity of sound at higher frequencies, resulting from a smaller main lobe in the beam pattern, the detection gets possible for tiny sound sources. Fig. 8 shows the maximum recorded 5 dB instead of the previously shown 3 dB to increase the visibility range at high frequencies. Of course, the maximum detected sound pressure level decreases with decreasing leak size. The smallest leaks are only detected at the highest analyzed frequency band with a center frequency of 25 kHz. This indicates a relationship between the leak size and the analyzed frequency.
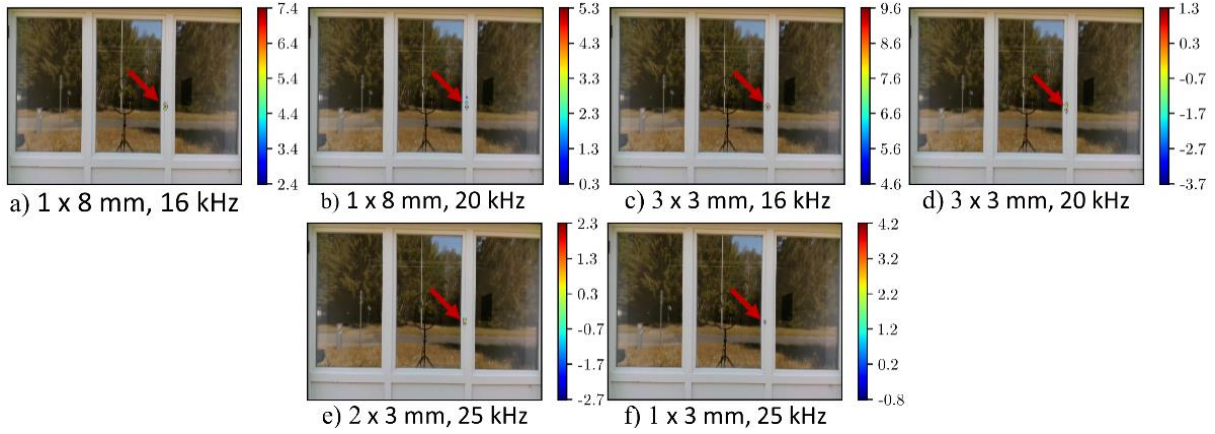
Figure 8 Acoustic images of selected third-octave frequency bands for the constructed leak of 1 x 8 mm, 3 x 3 mm, 2 x 3 mm, and 1 x 3 mm with superimposed sound pressure levels in dB and red arrows indicating the leaks

SUMMARY AND CONCLUSION

In this paper, a series of experiments assesses how artificially constructed leaks in a window façade are detected using an acoustic camera with a microphone ring array with 48 microphones. A broadband white noise sound source is placed inside the building. Six different configurations of constructed leaks simulate different degrees of a non-airtight window gasket. The location of all investigated leak sizes is detected with acoustic beamforming, particularly at frequencies >16 kHz. With decreasing leak size, the frequencies in which the leaks can be detected increase. The maximum detectable sound pressure level at these frequencies decreases with decreasing leak sizes. It is successfully demonstrated that the acoustic beamforming method is a viable method to detect and visualize leaks in the building envelope. The observed relationship between the leak size and the frequency range in which the leak can be detected shows the potential to give at least an estimate on the leak size. The tests are successful conducted for relatively simple leaks in a window gasket. More complex leaks, in particular longer leak paths, will be investigated in future work in real buildings to further assess the chances and limitations of the acoustic approach to leak detection. Infrared thermography, an established method for localization of leaks in building envelopes on site, detects heat bridges in addition to air leaks which may lead to a misinterpretation of the measurement results. On the other hand, measurements with the acoustic methods do not detect heat bridges but might be disturbed by surrounding noise. A combination of both can be promising for future work. Ongoing work (Kölsch et al. 2021) compares the results of the acoustic method for quantifying leaks to the established techniques of blower door tests and air change rate measurement with tracer gas.

NOMENCLATURE

$f(t)$	=	Time signals of sound pressure recorded at each microphone
$\hat{f}(\vec{x}, t)$	=	Reconstructed time signal at focus point $\vec{x}$
M	=	Number of microphones
n	=	Total number of discrete time samples
$\hat{p}_{rms}(\vec{x})$	=	Effective sound pressure at focus point
t	=	Time
$\vec{x}$	=	Focus point
Δ	=	Time delay
θ	=	Elevation angle

REFERENCES

Bi, Chuan-Xing, Yuan Liu, Yong-Bin Zhang, and Liang Xu. 2019. "Sound Field Reconstruction Using Inverse Boundary Element Method and Sparse Regularization." The Journal of the Acoustical Society of America 145 (5): 3154–62. https://doi.org/10.1121/1.5109393.

Billingsley, J., and R. Kinns. 1976. "The Acoustic Telescope." Journal of Sound and Vibration 48 (4): 485–510. https://doi.org/10.1016/0022-460X(76)90552-6.

Döbler, Dirk, and Christoph Puhle. 2015. "Correlation of High Channel Count Beamforming Measurement of a Car in a Wind Tunnel Using CLEAN-SC." In Proceedings of the 44th International Congress and Exposition on Noise Control Engineering, edited by Institute of Noise Control Engineering.

GFaI. 2020. NoiseImage, Version 4.12.2.17221: GFai Tech.

Grythe, Jorgen. 2015a. "Acoustic Camera and Beampattern." https://www.norsonic.de. Norsonic: Technical Note.

Grythe, Jorgen. 2015b. "Beamforming Algorithms - Beamformers." https://www.norsonic.de. Norsonic: Technical Note.

Herbordt, Wolfgang. 2005. Sound Capture for Human/Machine Interfaces: Practical Aspects of Microphone Array Signal Processing: Springer Berlin Heidelberg.

Jaeckel, Olaf. 2006. "Strengths and Weaknesses of Calculating Beamforming in the Time Domain." In Proceedings of the BeBeC, 8th Berlin Beamforming Conference, edited by Gesellschaft zur Förderung Angewandter Informatik.

Kölsch, Benedikt, Iain S. Walker, Björn Schiricke, William W. Delp, and Bernhard Hoffschmidt. 2021. "Quantification of Air Leakage Paths: A Comparison of Airflow and Acoustic Measurements." The International Journal of Ventilation. https://doi.org/10.1080/14733315.2021.1966576.

Maynard, J. D., E. G. Williams, and Y. Lee. 1985. "Nearfield Acoustic Holography: I. Theory of Generalized Holography and the Development of NAH." The Journal of the Acoustical Society of America 78 (4): 1395–1413. https://doi.org/10.1121/1.392911.

Moore, Brian C. 2004. An Introduction to the Psychology of Hearing. 5th ed. London, UK: Elsevier Academic Press.

Neugebauer, Stefan, Reinhard Rösel, and Dirk Döbler. 2014. "Correlation of Parallel Car Interior and Exterior Beamforming Measurements in a Wind Tunnel." In Proceedings of 43rd International Congress on Noise Control Engineering, edited by The Australian Acoustical Society.

Raman, Ganesh, Manisha Prakash, Rakesh Ramachandran, Hirenkumar Patel, and Kanthasamy Chelliah. 2014. "Remote Detection of Building Air Infiltration Using a Compact Microphone Array and Advanced Beamforming Methods." In Proceedings of the BeBeC, 5th Berlin Beamforming Conference, edited by Gesellschaft zur Förderung Angewandter Informatik.

Teutsch, Heinz. 2007. Modal Array Signal Processing: Principles and Application of Acoustic Wavefield Decomposition. Lecture Notes in Control and Information Sciences 348. Berlin Heidelberg: Springer.

Walker, Iain S., and David J. Wilson. 1998. "Field Validation of Algebraic Equations for Stack and Wind Driven Air Infiltration Calculations." HVAC&R Research 4: 119–39.